



HAL
open science

Multi-axial unsplit frequency-shifted perfectly matched layer for displacement-based anisotropic wave simulation in infinite domain

Zhinan Xie, Yonglu Zheng, Paul Cristini, Xubin Zhang

► To cite this version:

Zhinan Xie, Yonglu Zheng, Paul Cristini, Xubin Zhang. Multi-axial unsplit frequency-shifted perfectly matched layer for displacement-based anisotropic wave simulation in infinite domain. *Earthquake Engineering and Engineering Vibration*, 2023, 22 (2), pp.407-421. 10.1007/s11803-023-2170-3. hal-04292750

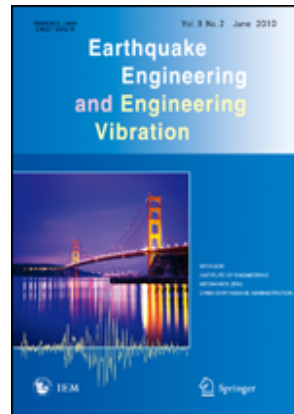
HAL Id: hal-04292750

<https://hal.science/hal-04292750>

Submitted on 17 Nov 2023

HAL is a multi-disciplinary open access archive for the deposit and dissemination of scientific research documents, whether they are published or not. The documents may come from teaching and research institutions in France or abroad, or from public or private research centers.

L'archive ouverte pluridisciplinaire **HAL**, est destinée au dépôt et à la diffusion de documents scientifiques de niveau recherche, publiés ou non, émanant des établissements d'enseignement et de recherche français ou étrangers, des laboratoires publics ou privés.



Multi-axial unsplit frequency-shifted perfectly matched layer for displacement-based anisotropic wave simulation in infinite domain

| | |
|------------------|--|
| Journal: | <i>Earthquake Engineering and Engineering Vibration</i> |
| Manuscript ID | EEEEV-21-213.R1 |
| Manuscript Type: | Original Article |
| Keywords: | Computational seismology, Seismic anisotropy, Wave propagation, Elastodynamics |
| Specialty Area: | Observation and analysis of ground motions < Engineering Seismology, Seismic hazard analysis and zonation < Engineering Seismology |
| | |

SCHOLARONE™
Manuscripts

Multi-axial unsplit frequency-shifted perfectly matched layer for displacement-based anisotropic wave simulation in infinite domain

Zhinan Xie

Email: wla_2012@163.com

Affiliation: Key Laboratory of Earthquake Engineering and Engineering Vibration, Institute of Engineering Mechanics, China Earthquake Administration; Key Laboratory of Earthquake Disaster Mitigation, Ministry of Emergency Management.
Harbin 150080, PR China

Yonglu Zheng

Email: iemzyl07@163.com

Affiliation: Key Laboratory of Earthquake Engineering and Engineering Vibration, Institute of Engineering Mechanics, China Earthquake Administration; Key Laboratory of Earthquake Disaster Mitigation, Ministry of Emergency Management.
Harbin 150080, PR China

Paul Cristini

Email: cristini@lma.cnrs-mrs.fr

Affiliation: Aix Marseille Univ., CNRS, Centrale Marseille, LMA
F-13353 Marseille Cedex 13, France

Xubin Zhang

Email: zhangxvbin.hebi@163.com

Affiliation: Key Laboratory of Earthquake Engineering and Engineering Vibration, Institute of Engineering Mechanics, China Earthquake Administration; Key Laboratory of Earthquake Disaster Mitigation, Ministry of Emergency Management.
Harbin 150080, PR China

Corresponding author:

Name: Zhinan Xie

Telephone Number: +86-15114557253

Email: wla_2012@163.com

Postal Address: Institute of Engineering Mechanics, China Earthquake Administration, Room #326, Xuefu Road #29, Harbin, Heilongjiang Province, 150080, PR China

SUMMARY

Multi-axial perfectly matched layer (M-PML), known to have lost the perfect-matching property owing to multi-axial coordinate stretching, has been numerically validated to be long-time stable and it is thus used extensively in linear anisotropic wave simulation and in isotropic cases where the PML becomes unstable. We are concerned with the construction of the M-PML for anisotropic wave simulation on basis of second order wave equation implemented with displacement-based numerical method. We address the benefit of the incorrect chain rule implicitly adopted in the previous derivation of the M-PML. We show that using the frequency-shifted stretching function improves the absorbing efficiency of the M-PML for near-grazing incident waves. Then, through multi-axial complex-coordinate stretching the second order anisotropic wave equation in weak form, we derive a time-domain multi-axial unsplit frequency-shifted PML (M-UFSPML) using the frequency-shifted stretching function and the incorrect chain rule. A new approach is provided to reduce the number of memory variables needed for computing convolution terms in the M-UFSPML. The obtained M-UFSPML is well suited for implementation with a finite element or spectral element method. By providing several typical examples, we verify numerically the accuracy and long-time stability of the implementation of our M-UFSPML with Legendre spectral element method.

Keywords: Computational seismology; Seismic anisotropy; Wave propagation; Elastodynamics

1. INTRODUCTION

Linear elastic anisotropy is common to wave propagation in the Earth's interior (Babuška & Cara 1991; Savage, 1999; Deuss *et al.* 2010; Almqvist & Mainprice, 2017) and its ice cover (Diez & Eisen, 2015; Sayers, 2018). Such anisotropy can be caused by factors such as a preferred orientation of crystals, aligned inclusions, or regular sequences of thin layers (Cerveny, 2005). In anisotropic media, seismic wave speeds depend on the local directions of wave propagation and wave polarization. In recent years, wave simulation integrated as part of adjoint seismic full-waveform tomography has increasingly been used in investigating the regional-scale anisotropic structure of the Earth (Zhu *et al.*, 2017).

In wave simulation, taking anisotropy into account makes it difficult to establish stable techniques for infinite domain truncation (Komatitsch *et al.* 2000). It is now well-known that Perfectly Matched Layer (PML; Bérenger, 1994) is intrinsically unstable for certain types of anisotropic medium (Bécache *et al.* 2003). Such instability is irrelevant to the type of complex coordinate stretching function used in deriving the PML and the PML formulation, such as a split, unsplit or auxiliary differential PML formulation derived for either the velocity-stress-based wave equation in first-order form or the displacement-based wave equation in second-order form (Komatitsch & Martin, 2007, Ping *et al.* 2014).

In the first-order case, Meza-Fajardo & Papageorgiou (2008) proposed an approach to stabilize the split PML and produce what is referred to as a multi-axial PML (M-PML) in anisotropic-wave simulation. Zeng *et al.* (2011) showed that the M-PML can stabilize wave simulation for a horizontally layered isotropic solid medium having a high Poisson ratio. In the M-PML, aside from damping in the direction normal to interfaces between the M-PML and the truncated domain, additional nonzero damping in tangential directions is introduced. Although the tangential damping is usually set to be much smaller than the normal damping, an important drawback is that the M-PML is not perfectly matched (Dmitriev & Lisitsa, 2011). Therefore, the M-PML can be interpreted as a compromise between the PML and absorbing layers with the same level of tangential and normal damping (Cerjan *et al.*, 1985; Sochacki *et al.*, 1987; Semblat *et al.*, 1987; Halpern *et al.*, 2011). To achieve the same level of accuracy, M-PML is more often more computationally efficient than standard absorbing layers but less efficient than PML. Gao & Huang (2017) developed a numerical algorithm to determine optimally the level of tangential damping.

The first-order M-PML cannot be directly used in the second-order wave equation

1
2
3 simulation with displacement-based numerical simulation methods, such as the finite element
4 (FE) method (e.g., Bao *et al.*, 1998), spectral element (SE) method (e.g., Komatitsch &
5 Tromp, 1999) and some finite difference methods (e.g., Moczo *et al.*, 2002). Festa & Vilotte
6 (2005) showed how to couple the first-order split PML, implemented with the staggered finite
7 difference method, into the second-order wave equation implemented with the FE/SE method
8 and Newmark-beta time-stepping scheme, using the equivalence between the Newmark
9 time-stepping scheme and the midpoint difference rule. Following Festa & Vilotte's
10 observation, Martin, Komatitsch and Gedney (2008) extended the first-order convolutional
11 frequency-shifted PML to the multi-axial case and then coupled it into the second-order wave
12 equation simulation with the SE method and Newmark-beta time-stepping scheme. Such
13 coupling remains an open problem in the case that other time-stepping schemes are used (Liu
14 & Zhang, 2019).

15
16 Following the idea of Meza-Fajardo & Papageorgiou (2008), several second-order
17 M-PMLs have been derived via multi-axial coordinate stretching the second-order wave
18 equation. Li & Bou (2010) developed a second-order convolutional frequency-shifted
19 M-PML in the frequency domain. In principle, Li & Bou's formulation is not fit for layered
20 heterogenous infinite-domain truncation because Li and Bou treated the gradient of all
21 convolutional terms in stress as additional body forces. Ping *et al.* (2014, 2016) extended the
22 second-order split PML proposed by Komatitsch & Tromp (2003) to the multi-axial case. The
23 formulation of Ping *et al.* (2014, 2016) inherited the shortcomings of the PML of Komatitsch
24 & Tromp (2003) arising from the introduced hybrid second-order and third-order ordinary
25 differential equations. The number of split displacement variables is at least five times that of
26 the original variables (Ma & Liu, 2006). Moreover, Ping *et al.* (2014, 2016) obtained an
27 inconsistent result that unlike the obtained M-PML with a damping parameter defined in the
28 high-order polynomial profile, the M-PML with a damping parameter defined in the
29 commonly used second-order polynomial profile loses its stability in long-time simulation.
30 Fathi *et al.* (2015) showed without theoretical justification that though the chain rule
31 prevalently used in the M-PML derivation is incorrect, the resulting M-PML performed better
32 than the M-PML derived with the corrected chain rule.

33
34 In this paper, we develop a second-order multi-axial unsplit frequency-shifted PML
35 (M-UFSPML). We firstly show the importance of introducing the non-rigorous chain rule for
36 stabilize M-UFSPML and the introduce of frequency-shifted coordinate stretching can also
37 improve the absorbing efficiency of the M-PML. We then derive the M-UFSPML by
38 multi-axial complex-coordinate stretching the second-order wave equation in weak form,
39 instead of the strong wave equation, to avoid possible improper matching between the
40 obtained PML wave equation and boundary or interface conditions. The improper matching is
41 an important mechanism that leads to an unstable PML (Duru & Kreiss, 2014). We introduce
42 a new way to reduce the number of memory variables needed for dealing with the
43 computation of convolution terms. The obtained M-UFSPML is in weak form and thus ready
44 for implementation using the FE/SE method. We verify numerically the accuracy and
45 long-time stability of the M-UFSPML through theoretical and practical applications in wave
46 simulation with the high-order Legendre spectral element method and explicit time-stepping
47 scheme.

50 2. NOTES ON THE CHOICE OF MULTI-AXIAL COORDINATE STRETCHING

51 Dmitriev & Lisitsa (2011) showed that the loss of the perfectly matched property of
52 M-the PML is due to multi-axial coordinate stretching. On the basis of their work, we
53 investigate the effects of multi-axial coordinate stretching, frequency-shifted coordinate
54 stretching and the implicitly adopted incorrect chain rule on the absorbing efficiency of the
55 M-PML, which leads to a useful remark on our late M-PML derivation.

56 For the simplest wave simulation in $(x, y) \in R$, we specify the computation domain as
57 $\{x < 0, y \in R\}$. Within this domain, the wave equation is
58
59
60

$$\begin{bmatrix} i\omega\hat{u}_x \\ i\omega\hat{u}_y \\ i\omega\hat{p} \end{bmatrix} = \begin{bmatrix} 0 & 0 & -1/\rho \\ 0 & 0 & 0 \\ -\rho c^2 & 0 & 0 \end{bmatrix} \begin{bmatrix} \partial_x \hat{u}_x \\ \partial_x \hat{u}_y \\ \partial_x \hat{p} \end{bmatrix} + \begin{bmatrix} 0 & 0 & 0 \\ 0 & 0 & -1/\rho \\ 0 & -\rho c^2 & 0 \end{bmatrix} \begin{bmatrix} \partial_y \hat{u}_x \\ \partial_y \hat{u}_y \\ \partial_y \hat{p} \end{bmatrix}, \quad (1)$$

where ρ is the density, c the acoustic wave speed, u_x and u_y the displacements in x and y directions respectively, and p the pressure. A caret above a variable denotes a Fourier transformation. $i = \sqrt{-1}$ and ω is the circular frequency. Following Meza-Fajardo & Papageorgiou (2008), we introduce complex coordinates in $\{x \geq 0, y \in R\}$ as

$$\mathcal{X}(x, y) = x + \int_0^x [d(x)/[\alpha(x) + i\omega]] dx', \quad \mathcal{Y}(x, y) = [1 + p^{y/x} d(x)/[\alpha(x) + i\omega]] y, \quad (2)$$

where $d(x)$ is the damping profile in the x direction and the constant $p^{y/x}$ refers to the level of additionally introduce damping in the y direction. $\alpha(x)$ serves to enhance the attenuation of evanescent and near-grazing waves and was set to zero by Meza-Fajardo & Papageorgiou (2008). With the incorrect chain rules given by Meza-Fajardo & Papageorgiou (2008), we obtain

$$d\mathcal{X} = s_x dx, \quad d\mathcal{Y} = s_y dy, \quad d\mathcal{X}d\mathcal{Y} = s_x s_y dx dy, \quad \partial_{\mathcal{X}} = (1/s_x) \partial_x, \quad \partial_{\mathcal{Y}} = (1/s_y) \partial_y, \quad (3)$$

where $s_x = 1 + d(x)/[\alpha(x) + i\omega]$ and $s_y = 1 + p^{y/x} d(x)/[\alpha(x) + i\omega]$ denote the coordinate stretching factor. We obtain the frequency-shifted M-PML by first mapping Eq. (1) to complex coordinates and then transforming to real coordinates using (3):

$$\begin{bmatrix} i\omega\hat{u}_x \\ i\omega\hat{u}_y \\ i\omega\hat{p} \end{bmatrix} = \begin{bmatrix} 0 & 0 & -1/(\rho s_x) \\ 0 & 0 & 0 \\ -\rho c^2/s_x & 0 & 0 \end{bmatrix} \begin{bmatrix} \partial_x \hat{u}_x \\ \partial_x \hat{u}_y \\ \partial_x \hat{p} \end{bmatrix} + \begin{bmatrix} 0 & 0 & 0 \\ 0 & 0 & -1/(\rho s_y) \\ 0 & -\rho c^2/s_y & 0 \end{bmatrix} \begin{bmatrix} \partial_y \hat{u}_x \\ \partial_y \hat{u}_y \\ \partial_y \hat{p} \end{bmatrix}. \quad (4)$$

However, because s_y depends on the variable x , in the corrected sense, the chain rule should be written as

$$d\mathcal{X} = s_x dx, \quad d\mathcal{Y} = \bar{s}_x dx + s_y dy, \quad d\mathcal{X}d\mathcal{Y} = s_x s_y dx dy, \quad \partial_{\mathcal{X}} = \frac{1}{s_x} \partial_x, \quad \partial_{\mathcal{Y}} = -\frac{\bar{s}_x}{s_x s_y} \partial_x + \frac{1}{s_y} \partial_y, \quad (5)$$

where $\bar{s}_x = y \partial_x s_y(x, y')$. Following the same process, the M-PML derived with Eq. (5) can be written as

$$\begin{bmatrix} i\omega\hat{u}_x \\ i\omega\hat{u}_y \\ i\omega\hat{p} \end{bmatrix} = \begin{bmatrix} 0 & 0 & -1/(\rho s_x) \\ 0 & 0 & \bar{s}_x/(\rho s_x s_y) \\ -\rho c^2(s_y - \bar{s}_x)/s_x s_y & 0 & 0 \end{bmatrix} \begin{bmatrix} \partial_x \hat{u}_x \\ \partial_x \hat{u}_y \\ \partial_x \hat{p} \end{bmatrix} + \begin{bmatrix} 0 & 0 & 0 \\ 0 & 0 & -1/(\rho s_y) \\ 0 & -\rho c^2/s_y & 0 \end{bmatrix} \begin{bmatrix} \partial_y \hat{u}_x \\ \partial_y \hat{u}_y \\ \partial_y \hat{p} \end{bmatrix}. \quad (6)$$

Following the plane-wave analysis presented by Dmitriev & Lisitsa (2011), we obtain the same reflection coefficient along the interface of the M-PML presented in Eq. (4):

$$R(\theta, s_y) = \left| \frac{\cos \theta - \sqrt{1 - \sin^2 \theta / s_y^2}}{\cos \theta + \sqrt{1 - \sin^2 \theta / s_y^2}} \right|, \quad (7)$$

where $||$ denotes the absolute norm. The reflection coefficient along the interface of the M-PML presented in Eq. (6) is

$$R(\theta, s_y, \bar{s}_x) = \left| \frac{\cos \theta - \frac{\sin \theta \bar{s}_x + \sqrt{(\sin \theta)^2 (\bar{s}_x^2 + 4s_y \bar{s}_x - 4s_y^2) + 4s_y^3 (s_y - \bar{s}_x)}}{2s_y (s_y - \bar{s}_x)}}{\cos \theta + \frac{\sin \theta \bar{s}_x + \sqrt{(\sin \theta)^2 (\bar{s}_x^2 + 4s_y \bar{s}_x - 4s_y^2) + 4s_y^3 (s_y - \bar{s}_x)}}{2s_y (s_y - \bar{s}_x)}} \right|. \quad (8)$$

Taking the commonly used profile $\alpha(x)=0, d(x)=(3c/2L)(|x|/L)^2$ with $c=1500m/s$ and $L=10\times c/f_0$, Figure 1 shows the distributions of $R(\theta, s_y)$ and $R(\theta, s_y)-R(\theta, s_y, \bar{s}_x)$ evaluated at $x=L/2$ and $y=L/2$. The results show the clear loss of the perfect-matching property in the M-PML, particularly for a near-grazing incident wave. The M-PML derived using the incorrect chain rule performs almost the same as that derived with the corrected chain rule but performs better in the region around $\omega=0$. Moreover, we present in Figure 2 the distribution of $R(\theta, s_y)$ with the same set of parameters taking into account commonly used nonzero $\alpha(x)=3\pi f_0(1-|x|/L)$. The figure clearly shows that nonzero $\alpha(x)$ serves to improve the absorbing efficiency of the near-grazing incident wave. Thus, in the later construction of the second-order M-PML, we reuse the non-rigorous chain rule but take into account the nonzero $\alpha(x)$.

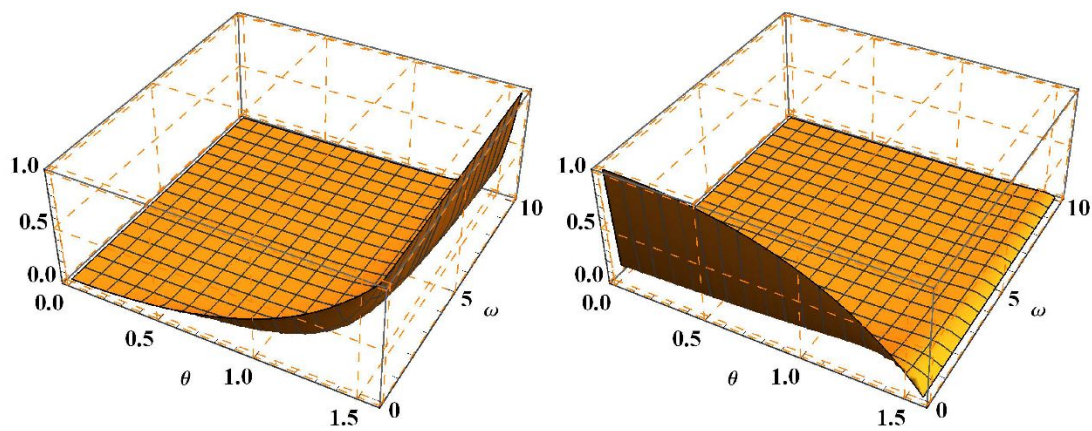


Figure 1. Distributions of $R(\theta, s_y)$ (left) and $R(\theta, s_y)-R(\theta, s_y, \bar{s}_x)$ (right) computed with $\alpha(x)=0$, $d(x)=(3c/2L)(|x|/L)^2$ ($c=1500m/s$, $L=10\times c/f_0$, $p^{y/x}=0.1$, $x=L/2$ and $y=L/2$).

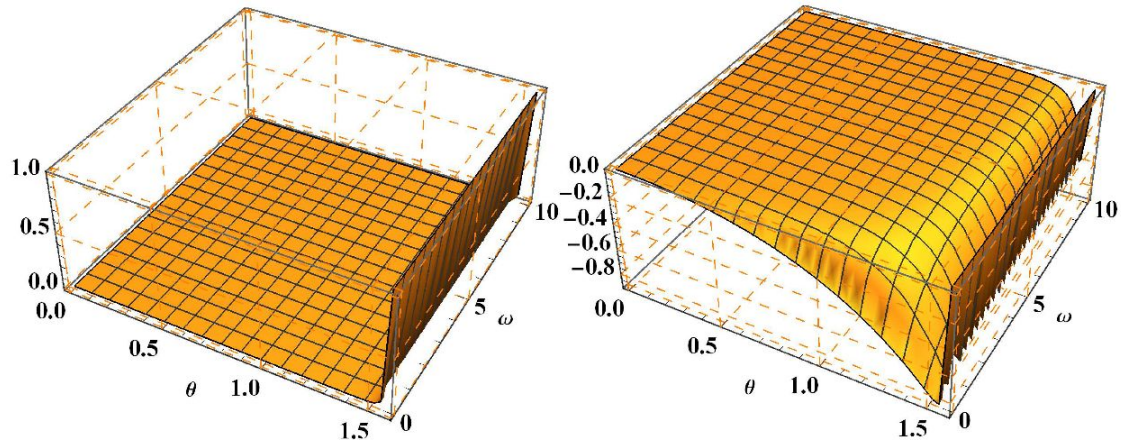


Figure 2. Distributions of $R(\theta, s_y)$ (left) computed with the same set of parameters as in Figure 1 except that $\alpha(x)=3\pi f_0(1-|x|/L)$ and the distribution of $R(\theta, s_y)|_{\alpha \neq 0} - R(\theta, s_y)|_{\alpha = 0}$ (right).

3. THE SECOND-ORDER M-UFSPML

By multi-axial complex stretching the second-order anisotropic wave equation in its weak form, we derive the second-order M-UFSPML with the incorrect chain rule and frequency-shifted coordinate stretching function. Moreover, we introduce a new way to approximately halve the memory cost in handling the computation of convolution terms via memory variables. At the end of the section, we summarize M-PML formulations and the number of additional memory variables needed in their implementation.

3.1. Second-order anisotropic wave equation

Following the matrix notation used by Carcione (2015), the second-order anisotropic wave equation can be written as

$$\rho \frac{\partial^2 \mathbf{u}}{\partial t^2} = \nabla \cdot \boldsymbol{\sigma} + \mathbf{f}, \quad (9)$$

where $\mathbf{u} = [u_x \ u_y \ u_z]^T = [u_1 \ u_2 \ u_3]^T$ and $\mathbf{f} = [f_1 \ f_2 \ f_3]^T$ are respectively vectors of the displacement and body force and $\boldsymbol{\sigma} = [\sigma_{xx} \ \sigma_{yy} \ \sigma_{zz} \ \sigma_{yz} \ \sigma_{xz} \ \sigma_{xy}]^T = [\sigma_1 \ \sigma_2 \ \sigma_3 \ \sigma_4 \ \sigma_5 \ \sigma_6]^T$,

$$\boldsymbol{\sigma} = \mathbf{C} \cdot \mathbf{e} = \mathbf{C} \cdot \nabla^T \cdot \mathbf{u}, \quad \nabla = \begin{pmatrix} \partial_1 & 0 & 0 & 0 & \partial_3 & \partial_2 \\ 0 & \partial_2 & 0 & \partial_3 & 0 & \partial_1 \\ 0 & 0 & \partial_3 & \partial_2 & \partial_1 & 0 \end{pmatrix}. \quad (10)$$

Here, $\mathbf{e} = [e_{xx} \ e_{yy} \ e_{zz} \ e_{yz} \ e_{xz} \ e_{xy}]^T = [e_1 \ e_2 \ e_3 \ e_4 \ e_5 \ e_6]^T$ and \mathbf{C} is the elasticity matrix. Let us restrict ourselves to the anisotropic medium with orthorhombic symmetry, which plays the most important role in seismology and seismic exploration. It covers the isotropic medium and anisotropic medium of VTI (vertical transverse isotropy) symmetry, HTI (Horizontal Transverse Isotropy) symmetry and the hexagonal symmetry. The elasticity matrix of an orthorhombic medium reads

$$\mathbf{C} = \begin{pmatrix} c_{11} & c_{12} & c_{13} & 0 & 0 & 0 \\ c_{12} & c_{22} & c_{23} & 0 & 0 & 0 \\ c_{13} & c_{23} & c_{33} & 0 & 0 & 0 \\ 0 & 0 & 0 & c_{44} & 0 & 0 \\ 0 & 0 & 0 & 0 & c_{55} & 0 \\ 0 & 0 & 0 & 0 & 0 & c_{66} \end{pmatrix}. \quad (11)$$

In the two-dimensional case (having x - y Cartesian coordinates), the in-plane wave equation can be obtained by simply omitting the variables and the spatial variation related to the z coordinate. We then have $\mathbf{u} = [u_1 \ u_2]^T$, $\boldsymbol{\sigma} = [\sigma_1 \ \sigma_2 \ \sigma_6]^T$, $\mathbf{e} = [e_1 \ e_2 \ e_6]^T$,

$$\nabla = \begin{pmatrix} \partial_1 & 0 & \partial_2 \\ 0 & \partial_2 & \partial_1 \end{pmatrix}, \text{ and } \mathbf{C} = \begin{pmatrix} c_{11} & c_{12} & 0 \\ c_{12} & c_{22} & 0 \\ 0 & 0 & c_{66} \end{pmatrix}. \quad (12)$$

3.2. DERIVATION OF THE SECOND-ORDER M-UFSPML

The PML is derived classically through complex coordinate stretching of the wave equation written in strong form. Recently, the weak-form approach for the PML derivation has been introduced. In the weak-form approach, the PML is derived through the complex coordinate stretching of the wave equation written in weak form (Bindel & Govindjee, 2005; Matuszyk & Demkowicz, 2013; Xie & Zhang, 2017). In the classical way, the derivation of the wave equation in the PML and that of the boundary and/or interface conditions are independent, and the two may be improperly matched, which can lead to numerical instability and reduced numerical accuracy as shown by Duru & Kreiss (2014). However, in taking the weak-form approach, such a mismatch can be naturally avoided because the free and interface conditions are simultaneously stretched in a consistent way. In the following sections, we derive the second-order M-UFSPM using the weak-form approach. We start from the second-order wave equation in weak form specified in the infinite domain $\{x > 0, y > 0\}$, which is written as

$$\int_{\Omega} \rho (-\omega^2) (\hat{u}_x w_x + \hat{u}_y w_y) dx dy + \int_{\Omega} (\partial_x w_x \hat{\sigma}_{xx} + \partial_y w_x \hat{\sigma}_{xy} + \partial_x w_y \hat{\sigma}_{yx} + \partial_y w_y \hat{\sigma}_{yy}) dx dy \\ = \int_{\Gamma} [(w_x \hat{\sigma}_{xx} + w_y \hat{\sigma}_{yx}) dy + (w_x \hat{\sigma}_{xy} + w_y \hat{\sigma}_{yy}) dx] \quad (13)$$

where Ω denotes the whole domain in $\{x > 0, y > 0\}$ and Γ represents the boundary of

Ω . Mapping Eq. (13) into complex coordinates defined by

$$\mathcal{X}(x, y) = x + \int_0^x \left\{ \frac{d(x) + p^{x/y} d(y)}{\alpha(x) + i\omega} \right\} dx' = x + \int_0^x \left\{ \frac{d_x^m}{\alpha_x + i\omega} \right\} dx', \quad (14)$$

$$\mathcal{Y}(x, y) = y + \int_0^y \left\{ \frac{p^{y/x} d(x) + d(y)}{\alpha(y) + i\omega} \right\} dy' = y + \int_0^y \left\{ \frac{d_y^m}{\alpha_y + i\omega} \right\} dy' \quad (15)$$

and transforming into the real coordinates using the incorrect chain rule (3), we get

$$\int_{\Omega} \rho \left(\frac{\partial_x w_x}{u_x} + \frac{\partial_y w_y}{u_y} \right) dx dy + \int_{\Omega} \left(\partial_x w_x \frac{\partial_x}{u_x} + \partial_y w_x \frac{\partial_y}{u_x} + \partial_x w_y \frac{\partial_x}{u_y} + \partial_y w_y \frac{\partial_y}{u_y} \right) dx dy \\ = \int_{\Gamma} \left[\left(w_x \frac{\partial_x}{u_x} + w_y \frac{\partial_y}{u_y} \right) dy + \left(w_x \frac{\partial_x}{u_x} + w_y \frac{\partial_y}{u_y} \right) dx \right] \quad (16)$$

$$\frac{\partial_x}{u_x} = (-\omega^2) s_x s_y \hat{u}_x, \quad \frac{\partial_y}{u_y} = (-\omega^2) s_x s_y \hat{u}_y, \quad (17)$$

$$\frac{\partial_{xx}}{u_x} = c_{11} (s_y/s_x) \partial_x \hat{u}_x + c_{12} \partial_y \hat{u}_y, \quad \frac{\partial_{yy}}{u_y} = c_{66} (s_x/s_y) \partial_y \hat{u}_x + c_{66} \partial_x \hat{u}_y, \quad (18)$$

$$\frac{\partial_{yx}}{u_x} = c_{66} \partial_y \hat{u}_x + c_{66} (s_y/s_x) \partial_x \hat{u}_y, \quad \frac{\partial_{xy}}{u_y} = c_{12} \partial_x \hat{u}_x + c_{22} (s_x/s_y) \partial_y \hat{u}_y, \quad (19)$$

where $s_x = 1 + d_x^m / (\alpha_x + i\omega)$ and $s_y = 1 + d_y^m / (\alpha_y + i\omega)$. The inverse Fourier transformations of $(-\omega^2) s_x s_y$, s_x/s_y , and s_y/s_x can be formally written as

$$F^{-1} \left[(-\omega^2) s_x s_y \right] = \delta(t) + a_0 \delta(t) + a_1 \delta(t) + a_2 e^{-\alpha_x t} H(t) + a_3 e^{-\alpha_y t} H(t), \quad (20)$$

$$F^{-1} \left[s_x/s_y \right] = \delta(t) + a_4 e^{-\alpha_x t} H(t) + a_5 e^{-(\alpha_y + d_y^m) t} H(t), \quad (21)$$

$$F^{-1} \left[s_y/s_x \right] = \delta(t) + a_6 e^{-\alpha_y t} H(t) + a_7 e^{-(\alpha_x + d_x^m) t} H(t). \quad (22)$$

The detailed expression of a_i , $i=1, \dots, 7$ can be found in Appendix B of the study of [Xie et al. \(2014\)](#). Substituting Eqs. (20)–(22) into (17)–(19), we get the time-domain M-UFSPML in weak form:

$$\int_{\Omega} \rho \left(\frac{\partial_x w_x}{u_x} + \frac{\partial_y w_y}{u_y} \right) dx dy + \int_{\Omega} \left(\partial_x w_x \frac{\partial_x}{u_x} + \partial_y w_x \frac{\partial_y}{u_x} + \partial_x w_y \frac{\partial_x}{u_y} + \partial_y w_y \frac{\partial_y}{u_y} \right) dx dy \\ = \int_{\Gamma} \left[\left(w_x \frac{\partial_x}{u_x} + w_y \frac{\partial_y}{u_y} \right) dy + \left(w_x \frac{\partial_x}{u_x} + w_y \frac{\partial_y}{u_y} \right) dx \right] \quad (23)$$

Taking $\frac{\partial_x}{u_x}$ as an example,

$$\frac{\partial_x}{u_x} = (-\omega^2) s_x s_y \hat{u}_x = \delta_x + a_0 u_x + a_1 u_x + a_2 \left[e^{-\alpha_x t} H(t) \right] * u_x + a_3 \left[e^{-\alpha_y t} H(t) \right] * u_x, \quad (24)$$

within which two convolution terms exist. To compute convolution terms, we need to introduce a memory variable such as $\psi(t) = \left[e^{-bt} H(t) \right] * g(t)$. Denoting the evaluation of $\psi(t)$ at $t_n = n\Delta t$ by ψ_n , ψ_{n+1} can be updated using the recursive convolution technique summarized by [Xie et al. \(2014\)](#). Thus, 12 memory variables are needed to deal with all convolution terms in the time-domain M-UFSPML. To reduce the number of memory variables, we restructure the M-UFSPML as

$$\int_{\Omega} \rho \left(\frac{\partial_x w_x}{u_x} + \frac{\partial_y w_y}{u_y} \right) dx dy + \int_{\Omega} \left(\partial_x w_x \frac{\partial_x}{u_x} + \partial_y w_x \frac{\partial_y}{u_x} + \partial_x w_y \frac{\partial_x}{u_y} + \partial_y w_y \frac{\partial_y}{u_y} \right) dx dy \\ = \int_{\Gamma} \left[\left(w_x \frac{\partial_x}{u_x} + w_y \frac{\partial_y}{u_y} \right) dy + \left(w_x \frac{\partial_x}{u_x} + w_y \frac{\partial_y}{u_y} \right) dx \right] \quad (25)$$

$$\frac{\partial_x}{u_x} = \delta_x + a_0 u_x + a_1 u_x + a_2 \bar{u}_x^{\alpha_x} + a_3 \bar{u}_x^{\alpha_y}, \quad \frac{\partial_y}{u_y} = \delta_y + a_0 u_y + a_1 u_y + a_2 \bar{u}_y^{\alpha_x} + a_3 \bar{u}_y^{\alpha_y}, \quad (26)$$

$$\frac{\partial_{ij}}{u_j} = \sigma_{ij} - d_j^m \bar{\sigma}_{ij}^{d_j^m + \alpha_j}, \quad i, j = x, y, \quad (27)$$

$$\sigma_{xx} = c_{11} \partial_x \left(u_x + d_x^m \bar{u}_x^{\alpha_x} \right) + c_{12} \partial_y \left(u_y + d_x^m \bar{u}_y^{\alpha_x} \right), \quad \sigma_{xy} = c_{66} \partial_y \left(u_x + d_x^m \bar{u}_x^{\alpha_x} \right) + c_{66} \partial_x \left(u_y + d_y^m \bar{u}_y^{\alpha_y} \right), \quad (28)$$

$$\sigma_{yx} = \sigma_{xy}, \quad \sigma_{yy} = c_{12} \partial_x \left(u_x + d_y^m \bar{u}_x^{\alpha_y} \right) + c_{22} \partial_y \left(u_y + d_y^m \bar{u}_y^{\alpha_y} \right), \quad (29)$$

where $\bar{u}_i^{\alpha_i} = \left[e^{-\alpha_i t} H(t) \right] * u_i(t)$, $\bar{\sigma}_{ij}^{d_j^m + \alpha_j} = \left[e^{-(d_j^m + \alpha_j) t} H(t) \right] * \sigma_{ij}(t)$, $i, j = x, y$. Through simple counting, we see that only eight memory variables are needed in the restructured

M-UFSPML. In the three-dimensional case, only 18 memory variables are needed in the restructured M-UFSPML, whereas in the original formulation, 39 memory variables are needed. However, in the case that $\alpha_i = 0$, the number of additionally needed memory variables in the M-UFSPML presented in Eqs. (25)–(29) is greater than that in the M-UFSPML presented in Eqs. (16)–(19), which is four in the two-dimensional case.

For comparison, we summarize the M-PML formulations and the number of additional variables needed for their implementation in time-domain elastodynamics in Table 1. The number listed in the table is the number of additional variables introduced in the M-PML relative to the wave equation in the computational domain. Notably, in the first-order case, there are five wave equations (two for velocities and three for stresses), whereas in the second-order case, there are two wave equations (two for displacements). The table thus shows that the memory cost is lowest for our formulation. Moreover, in their M-USFPML, Li & Bou (2010) treated the convolutional terms involving the divergence of stress, containing second-order space partial differentials, as body force terms. The direct computation of second-order space partial differentials in the FE or SE method requires a dense grid in the case that high-order (≥ 2) element interpolant functions are used and such computation could be wrong in the case of low-order (≤ 2) element interpolant functions (Zhebel *et al.*, 2014). The same problem exists for the first-order M-UFSPML given by Martin, Komatitsch and Gedney (2008). Thus, the M-UFSPML presented here is more suitable for implementation using FE/SE methods, irrespective of the order of element interpolants. The weak-form M-UFSPML shares the same structure as the weak-form wave equation, and the implementation of the M-UFSPML can thus use the same code as the wave equation except for the additional treatment of convolution within the element-wise stress and strain computation. The detailed implementation of the second-order wave equation was described by Komatitsch & Tromp (1999), and we do not repeat it in this paper.

4. NUMERICAL EXPERIMENTS

We present three numerical experiments to test the accuracy and long-time stability of our M-UFSPML formulation. The first example involves isotropic wave simulation in a homogeneous semi-infinite model. The second involves anisotropic wave simulations in a homogeneous infinite model. The third involves simulation using a horizontally layered model filled with coupled isotropic and anisotropic media. We compare the accuracy of our M-UFSPML against that of the extended-domain solution obtained by enlarging the truncated domain and other results obtained using different infinite-domain truncation techniques. A fixed-boundary condition (setting the displacement to zero) is applied along the outside boundary of the M-UFSPML.

Unless otherwise specified, in all experiments, we use a polynomial degree $N = 5$ for the Lagrange interpolants within each Legendre spectral element. For time-stepping, we use the second-order explicit Newmark scheme ($\beta = 0$, $\gamma = 1/2$) combined with a recursive convolution technique given in Eq. (73) of the paper of Xie *et al.* (2014). According to Collino & Tsogka (2001), the damping profile normal to the M-UFSPML interface is

$$d(x_i) = \frac{3V_{P,\max}}{2L} (|x_i|/L)^2, \quad (30)$$

where L is the thickness of the M-UFSPML, x_i is the distance along the normal direction measured from the interface, and $V_{P,\max}$ is the maximum velocity of the primary arriving wave in the media. Following Zhang & Shen (2010), we set

$$\alpha(x_i) = 3\pi f_0 (1 - |x_i|/L), \quad (31)$$

where f_0 is the dominant frequency of the source time function

$$R(t) = \left[1 - 2(\pi f_0 (t - t_0))^2 \right] e^{[-(\pi f_0 (t - t_0))^2]} \quad (32)$$

and t_0 is its onset time. We study the decay of energy with time throughout the domain to check the long-time stability of our formulation by evaluating the total energy, which is the sum of the kinetic and potential energies:

$$E = \frac{1}{2} \rho \|\mathbf{u}\|_2 + \frac{1}{2} \sum_e \sum_j \sigma_{lk}^{e,j} \varepsilon_{lk}^{e,j}, \quad (33)$$

where $\|\mathbf{u}\|_2$ is the norm of the velocity vector and $\sigma_{lk}^{e,j}, \varepsilon_{lk}^{e,j}$ are respectively the stress and strain components.

4.1 Isotropic wave simulation in semi-infinite domain

We consider a homogeneous isotropic semi-infinite model with a traction-free boundary at its top. The M-UFSPML is applied for infinite-domain truncation along the other three sides. The elastic properties of the medium and geometrical and discretization parameters of the model are listed in the second column of Table 2. Within the M-UFSPML, we set p^{xy} and p^{yx} equal to 0.1. Owing to the loss of the perfect-matching property of the M-UFSPML, we compare first the accuracy of the normalized displacement of the USFPML having a thickness of 300 m with that of the M-UFSPML having different thicknesses, namely 300, 900 and 1500 m, corresponding to 3, 9 and 15 elements, respectively. For the P wave, the respective ratios of the M-UFSPML thickness to the dominant wavelength are approximately 0.23, 0.70 and 1.17. For the S wave, the ratios are approximately equal to 0.40, 1.20 and 2.00. Figure 3 shows snapshots of the wavefield at 2, 4, and 8 s computed with the nine-element M-UFSPML and three-element UFSPML. Owing to the unified scale used for all snapshots, we do not see a clear difference between the snapshots obtained with the nine-element M-UFSPML and the three-element UFSPML. However, Figure 4, showing the time history of the normalized displacement at the receiver, reveals that the accuracy of the M-UFSPML increases with the thickness of the M-UFSPML but is always lower than that of the UFSPML. Only in the case of thickness of 15 elements is the accuracy of the M-UFSPML close to that of the UFSPML. The accuracy of the nine-element M-UFSPML is sufficiently fine for practical application. The M-UFSPML has no clear difference in its absorbing efficiency between body waves and Rayleigh waves. We compare the accuracy of the M-UFSPML in our paper with that of the M-UFSPML obtained by Li & Bou (2010), both having a thickness set as nine elements. Figure 5, comparing the time history of the displacement at the receiver, shows that the accuracy of the M-UFSPML is slightly better than that of the M-UFSPML obtained by Li & Bou (2010), referred to as the M-UFSPML-Li. Additionally, the accuracy of the M-UFSPML is better than that of the M-UPML within which $\alpha(x_i) = 0$ and the widely used first-order Stacey absorbing boundary condition (Stacey, 1988). To ensure a fair comparison, in the case that the Stacey absorbing boundary condition is used, the computation domain is extended to include the space occupied by the M-UFSPML.

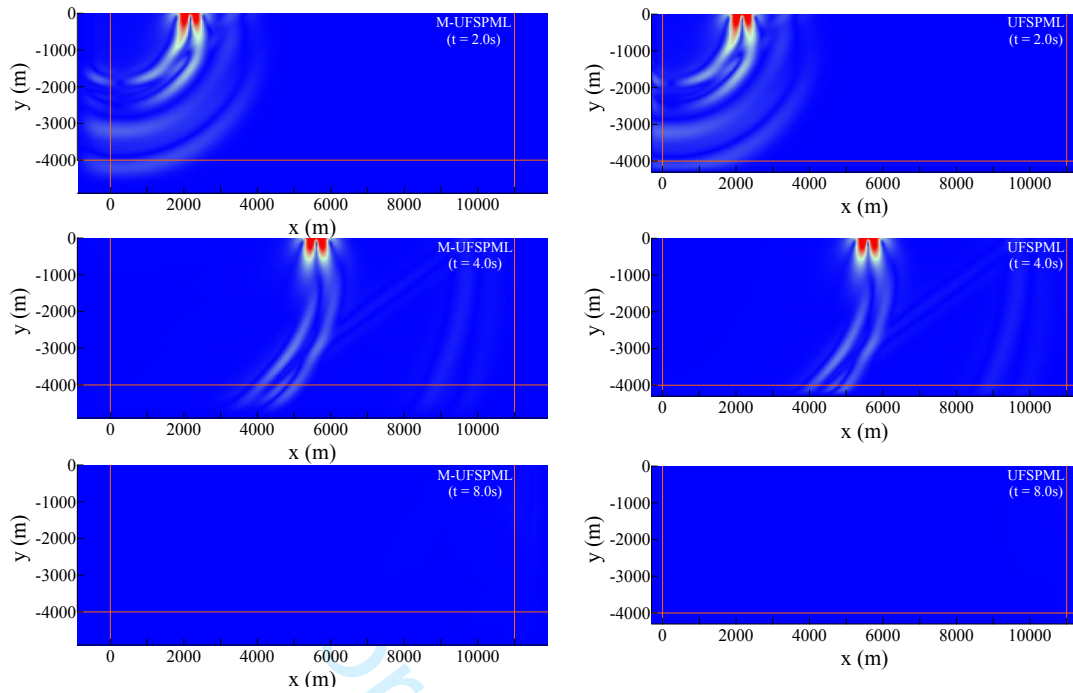


Figure 3. Snapshots of the normalized displacement $\sqrt{u_x^2 + u_y^2}$ taken at 2, 4, and 8 s, computed with different infinite-domain truncation techniques: (left column) M-UFSPML with a thickness of nine elements and (right column) UFSPML with a thickness of three elements (isotropic medium, semi-infinite model, vertical excitation).

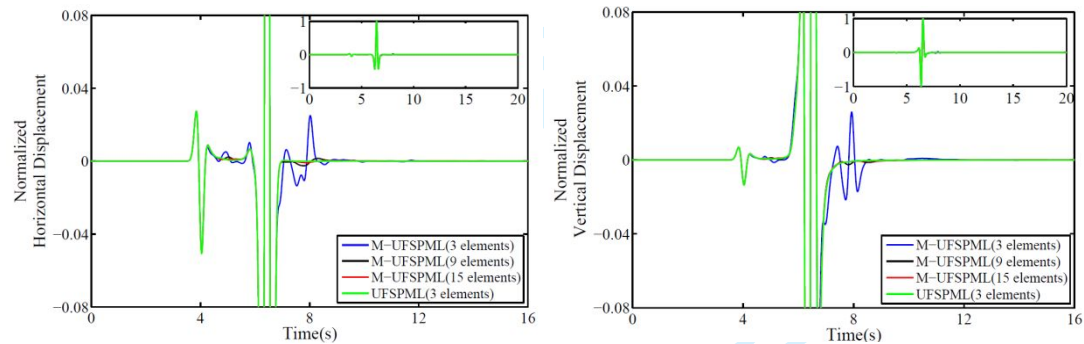


Figure 4. Comparison of time histories of the normalized horizontal and vertical displacements at the receiver computed with M-UFSPMLs having the thickness of 3, 9, and 15 elements and an UFSPML having thickness of three elements (isotropic medium, semi-infinite model, vertical excitation).

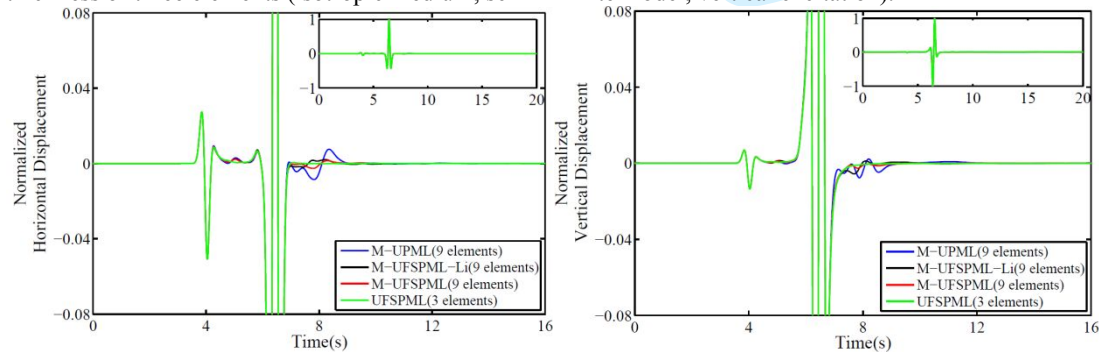


Figure 5. Comparison of time histories of the normalized horizontal and vertical displacements at the receiver computed with an M-UPML, M-UFSPML-Li, and M-UFSPML having thickness of nine elements and an UFSPML having thickness of three elements. M-UFSPML-Li refers to the result obtained with the M-UFSPML by Li & Bou (2010) (isotropic medium, semi-infinite model, vertical excitation).

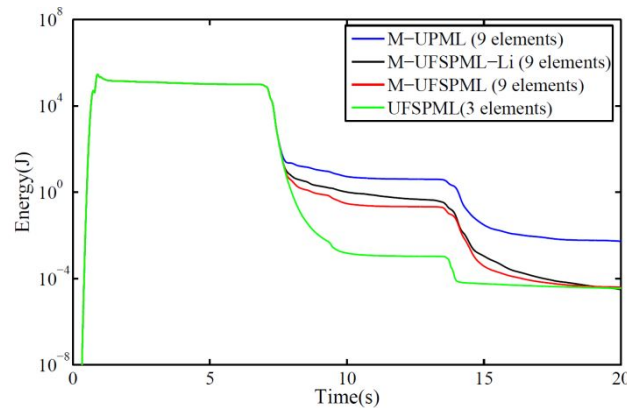


Figure 6. Total decay of energy throughout the domain computed with the M-UFSPML, M-UPML, and M-UFSPML-Li having thickness of nine elements and the UFSPML having thickness of three elements. M-UFSPML-Li refers to the result obtained with the M-UFSPML by [Li & Bou \(2010\)](#) (isotropic medium, semi-infinite model, vertical excitation).

4.2 Anisotropic wave simulation in infinite domain

We now consider the anisotropic wave simulation in homogeneous infinite domain. Three types of anisotropic medium are considered. The geometry and discretization parameters are given in the second and third columns of Table 2. The elastic properties of the anisotropic medium are given in Table 3. In all cases, we set $p^{x|y}$ and $p^{y|x}$ of the M-UFSPML equal to 0.1 except for anisotropic medium III, for which we use $p^{x|y} = p^{y|x} = 0.25$. For each case, we compare the absorbing efficiency of the M-UFSPML, of which the thickness is set uniformly as nine times the element size, with the efficiency of the standard Stacey ABC. The wave speed in the anisotropic medium depends on the azimuth, and the ratios of the M-UFSPML thickness to the dominate wavelength are thus different for waves having a different azimuth; that is, approximately 0.7 for primary arriving waves and 1.2 for secondary arriving waves. To ensure a fair comparison, in the case that the Stacey ABC is used, the computation domain is extended to include the space occupied by the M-UFSPML. In all cases, we first present snapshots of the normalized displacement at three different times for a vertical excitation. The left panel of Figure 7 shows waves at an evolving stage, whereas the center and right panels show the absorption of waves in the M-UFSPML region. In Figures 7, 9 and 11, there are no discernible reflections from the M-UFSPML interface, indicating satisfactory performance of the nine-element M-UFSPML. Figures 10, 12 and 14 compare the normalized horizontal and vertical displacement time histories at the receiver computed with the M-UFSPML, Stacey ABC and infinitely extended domain, the solution of which is referred to as an extended solution. We observe that fairly good absorbing efficiency is achieved with the nine-element M-UFSPML, which is less than 2% in the case of medium III and less than 1% in other cases. The excellent performance of the M-UFSPML is partially attributable to the non-grazing incident waves in all cases. Reflection can also be observed owing to the imperfect interface of the M-UFSPML. We therefore recommend using the UFSPML for an anisotropic medium with elastic properties, satisfying the sufficient conditions for PML stability given by [Bécache et al. \(2003\)](#).

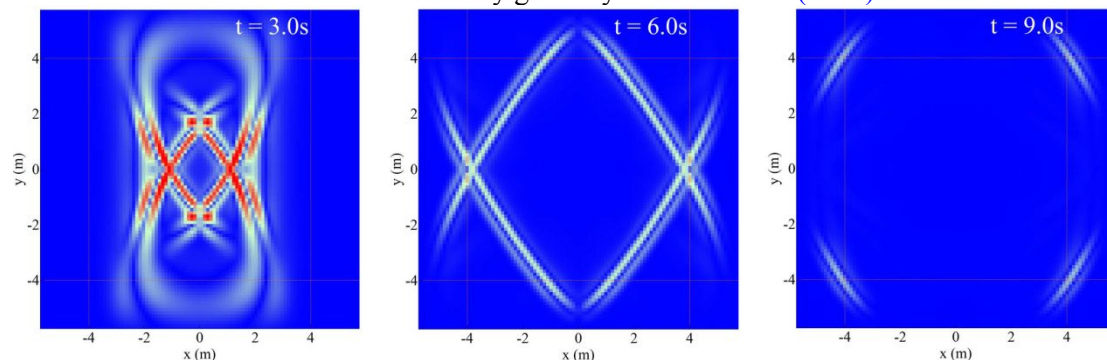


Figure 7. Comparison of snapshots of the normalized displacement $\sqrt{u_x^2 + u_y^2}$ taken at 3, 6, 9 s and computed with different infinite-domain truncation techniques: M-UFSPML having a thickness of nine elements (anisotropic medium III, infinite model, vertical excitation).

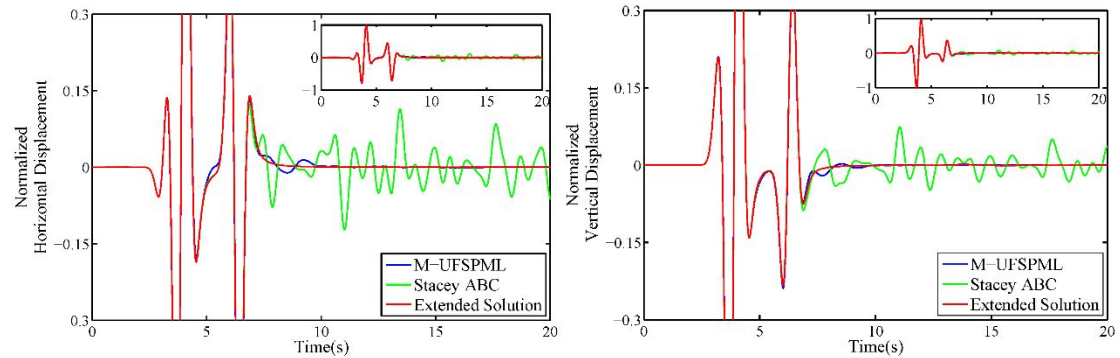


Figure 8. Comparison of time histories of the normalized horizontal and vertical displacements at the receiver computed with the M-UFSPML having thickness of nine elements, Stacey ABC and the extended domain (anisotropic medium III, infinite model, vertical excitation).

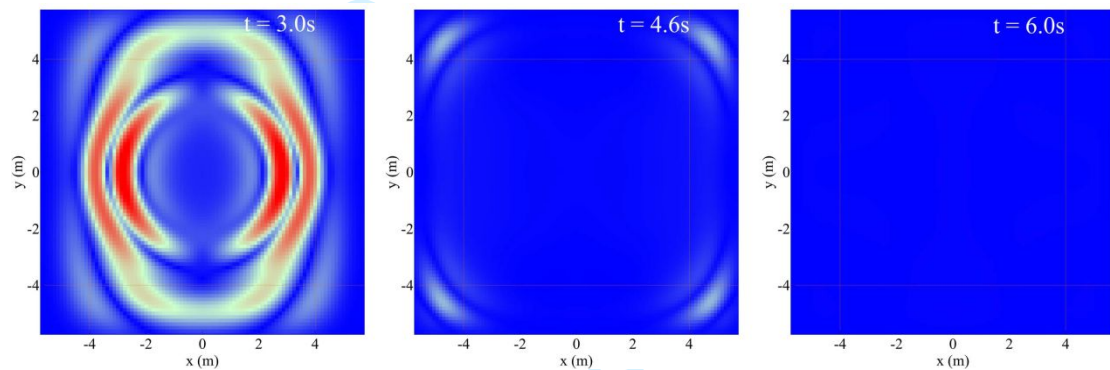


Figure 9. Comparison of snapshots of the normalized displacement $\sqrt{u_x^2 + u_y^2}$ taken at 3.0, 4.6, and 6.0 s and computed with different infinite-domain truncation techniques: M-UFSPML having thickness of nine elements (anisotropic medium IV, infinite model, vertical excitation).

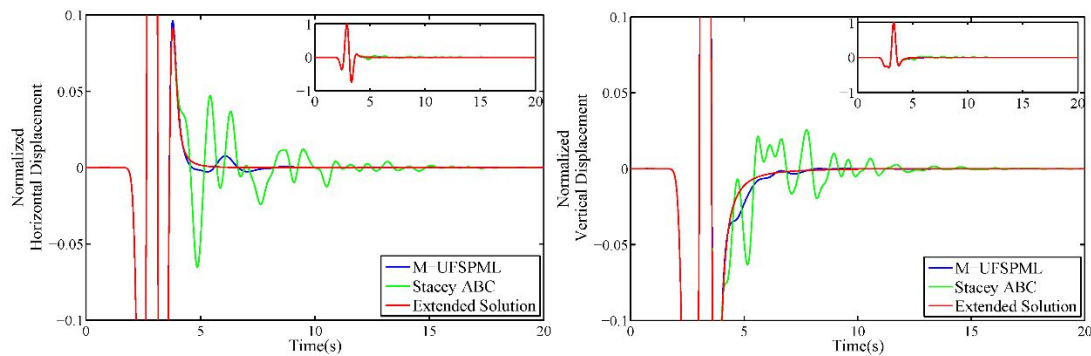


Figure 10. Comparison of time histories of normalized horizontal and vertical displacements at the receiver computed with M-UFSPML having thickness of nine elements, Stacey ABC and the extended domain (anisotropic medium IV, infinite model, vertical excitation).

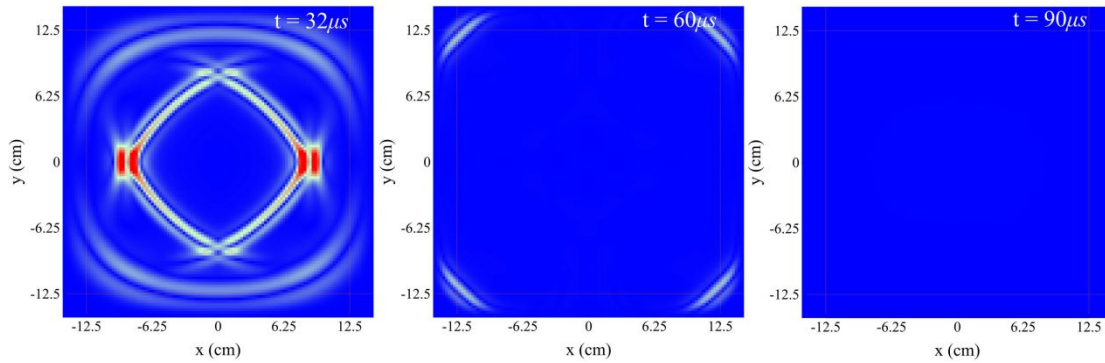


Figure 11. Comparison of snapshots of the normalized displacement $\sqrt{u_x^2 + u_y^2}$ taken at 32, 60, and 90 μs and computed with different infinite-domain truncation techniques: M-UFSPML having thickness of nine elements (anisotropic medium Apatite, infinite model, vertical excitation).

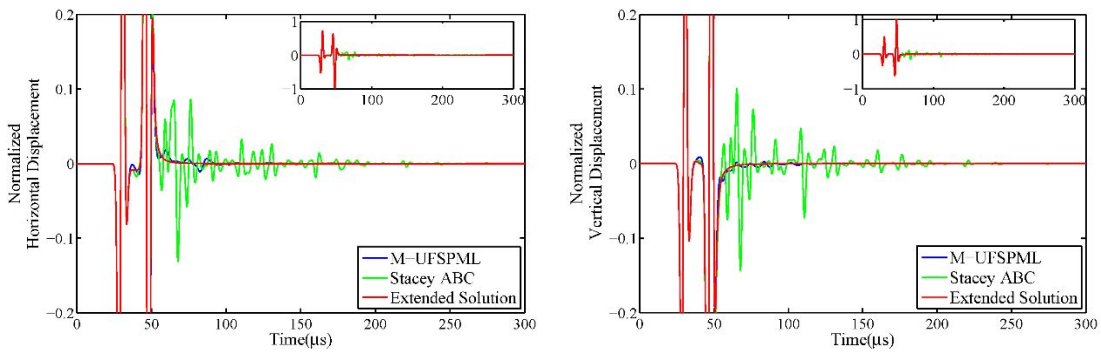


Figure 12. Comparison of normalized horizontal and vertical displacement time histories at the receiver computed with M-UFSPML of 9 elements size thickness, Stacey ABC and the extended domain (anisotropic medium apatite, infinite model, vertical excitation).

4.3. Coupled isotropic and anisotropic wave simulation in a layered model

We present the performance of the M-UFSPML in a heterogeneous medium. We consider a two-dimensional four-layer model adapted from the work of Zhu (2017) with the medium properties given in Table 4. The media in the first and fourth layers are isotropic. In the second layer, a medium having vertical transverse isotropy is considered. To consider the main anisotropic medium used in seismology, the medium in the third layer is set as a single set of vertical fractures embedded in an isotropic medium, resulting in horizontal transverse isotropy. The discretization parameters are given in Table 5. We set $p^{x|y}$ and $p^{y|x}$ of the M-UFSPML at 0.1 and the M-UFSPML thickness as nine elements. The wave speed in an anisotropic medium depends on the azimuth, and the ratios of the M-UFSPML thickness to the dominate wavelength thus differ between waves with different azimuth; that is, approximately 0.7 for primary arriving waves and 1.2 for secondary arriving waves. As shown in Figure 13, the M-UFSPML performs well in absorbing complex waves in the layered model. A long-time numerically stable simulation can be conducted. Figure 14 shows the energy decay curve for the entire domain containing the truncated computational domain and M-UFSPML. Additionally, we compare the energy decay curve computed with Stacey ABC and the M-UFSPML given by Li & Bou (2010), where the thickness is set to nine elements. The energy decay is quicker when our M-UFSPML is used owing to the better absorbing efficiency. However, from the time history of the two components of the normalized displacement at the receiver 100 m from the right of the M-UFSPML as shown in Figure 15, clear spurious reflections returning to the physical domain could be observed in all cases owing to near-grazing waves generated by multiple reflections and transmission. Finally, it is worth noting that the long penetration depth associated with surface waves must be considered to avoid their interference with the M-UFSPML. The same problem exists for PML application. Xie *et al.* (2016) illustrated that for PML application in wave simulation within an elastic Pekeris waveguide, when surface waves interfere with the PML, the absorbing efficiency of the PML decreases and cannot be improved by simply increasing the

thickness of the PML.

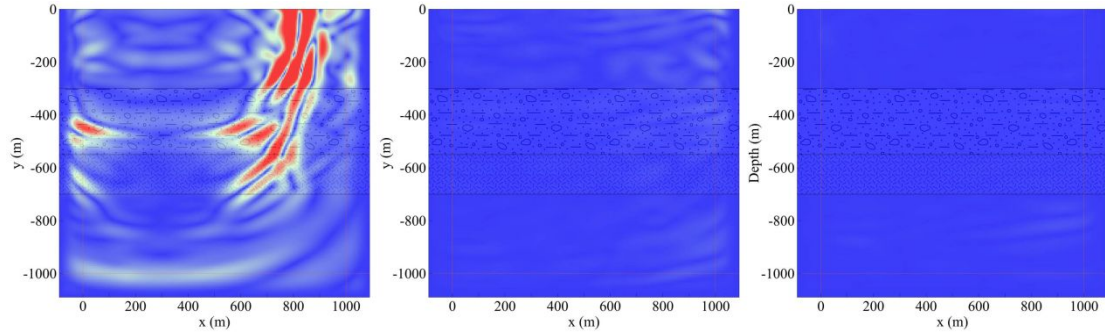


Figure 13. Comparison of snapshots of the normalized displacement $\sqrt{u_x^2 + u_y^2}$ taken at 0.6 s (left), 1.2 s (center), and 1.8 s (right) computed with different infinite-domain truncation techniques: M-UFSPML having thickness of nine elements (coupled isotropic and anisotropic medium, layered model, vertical excitation).

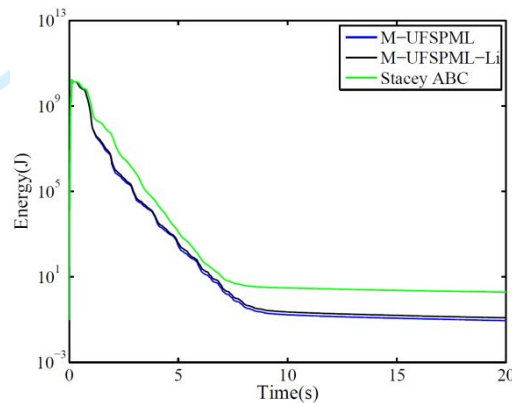


Figure 14. Total decay of energy throughout the domain computed with the M-UFSPML, M-UFSPML-Li having thickness of nine elements and Stacey ABC (coupled isotropic and anisotropic medium, layered model, vertical excitation). M-UFSPML-Li refers to the result obtained with the M-UFSPML by Li & Bou (2010).

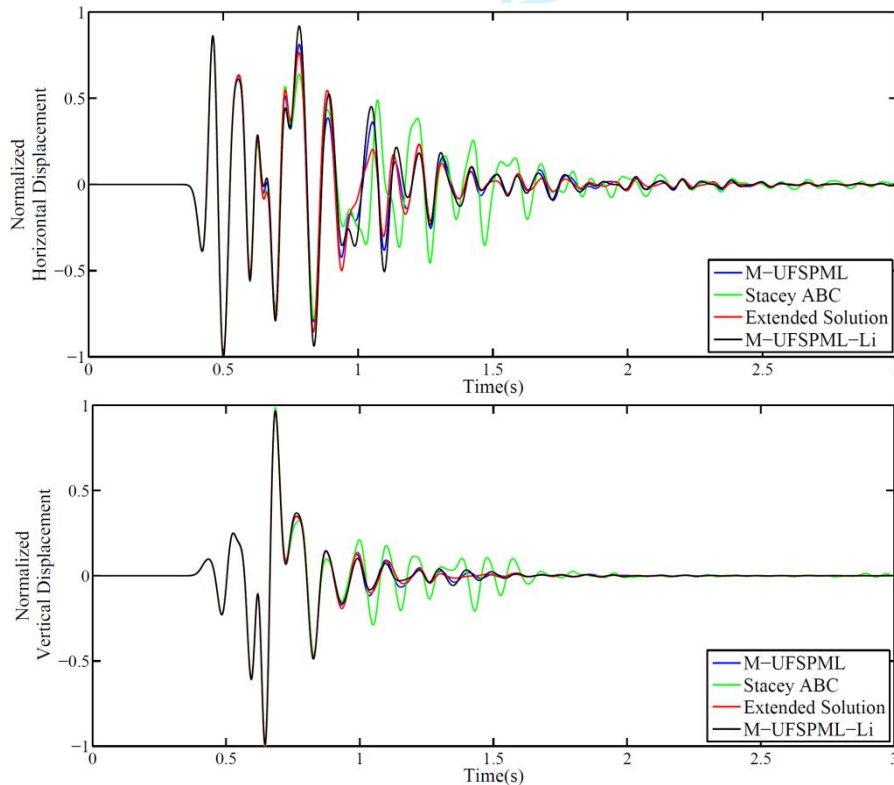


Figure 15. Comparison of time histories of normalized horizontal and vertical displacements at the receiver

1
2
3 computed with the M-UFSPML, M-UFSPML-Li with thickness of nine elements, Stacey ABC and the
4 extended solution (coupled isotropic and anisotropic medium, layered model, vertical excitation).
5 M-UFSPML-Li refers to the result obtained with the M-UFSPM by [Li & Bou, \(2010\)](#).
6

7 **5. CONCLUSIONS**

8 We developed a second-order M-UFSPML for infinite-domain truncation in the
9 simulation of a linear anisotropic wave. Using plane wave analysis, we validate the
10 importance of the usage of the non-rigorous chain rules in Meza-Fajardo & Papageorgiou
11 (2008), which has not been addressed before. The non-rigorous chain rules, instead of the
12 rigorous ones, lead to the improve absorbing efficiency of M-PML for low frequency incident
13 waves, which is importance for low-frequency seismic wave simulation adopted in seismic
14 hazard analysis. Moreover, we show the importance of complex frequency-shifted stretching
15 function can also improve the absorbing efficiency of M-PML for near-grazing incident
16 waves. Based on above inspection, Our M-UFSPML is derived through the multi-axial
17 complex stretching of the second-order anisotropic wave equation written in its weak form.
18 The formulation readily works with standard displacement-based FE and SE wave simulation
19 with only minor modification of the code in the computational domain. It is simple to
20 implement and allows for a natural application of traction-free boundary conditions or
21 interface conditions. The accuracy and long-time stability of the formulation was
22 demonstrated using high-order SE discretization with a second-order explicit Newmark time
23 integrator, which showed the accuracy of the method and its ability to solve wave propagation
24 in anisotropic media having orthorhombic symmetry. Although the interface of the M-PML is
25 not perfectly matched, it remains more efficient at absorbing both body waves and interface
26 waves than low-order absorbing boundary conditions such as the widely used Stacey ABC in
27 engineering. One topic of interest for future study would be to extend this work to forward
28 and adjoint wave simulation in anisotropic viscoelastic media ([Carcione, 2015](#)). Another topic
29 of interest for future studies would be to set up a community model for accurate comparison
30 of the computational efficiency of different infinite-domain truncation technologies (e.g., [Liao
31 et al., 1984](#), [Panji et al., 2014](#); [Zhao et al., 2018](#)).
32
33

34 **ACKNOWLEDGEMENTS**

35
36 This study was funded by Scientific Research Fund of Institute of Engineering Mechanics,
37 China Earthquake Administration (No. 2021EEVVL0102), National Natural Science
38 Foundation of China (No. U2039209; 51808516) and the National Key R&D Program of
39 China (No. 2018YFC1504004), Distinguished Young Scholars Program of the Natural
40 Science Foundation of Heilongjiang province, China (No. YQ2020E005). Zhinan mourn for
41 Dimitri Komatitsch, a visionary computational geophysicist and a great teacher.
42

43 **REFERENCES**

- 44
45 Almquist, B.S. & Mainprice, D., 2017. Seismic properties and anisotropy of the continental
46 crust: Predictions based on mineral texture and rock microstructure, *Reviews of
47 Geophysics*, 55(2), 367-433.
48 Babuška, V. & Cara, M., 1991. *Seismic anisotropy in the Earth (Vol. 10)*, Springer Science &
49 Business Media.
50 Bao, H., Bielak, J., Ghattas, O., Kallivokas, L.F., O'Hallaron, D.R., Shewchuk, J.R. & Xu, J.,
51 1998. Large-scale simulation of elastic wave propagation in heterogeneous media on
52 parallel computers, *Computer Methods in Applied Mechanics and Engineering*,
53 152(1-2), 85-102.
54 Bécache, E., Fauqueux, S. & Joly, P., 2003. Stability of perfectly matched layers, group
55 velocities and anisotropic waves, *Journal of Computational Physics*, 188(2), 399-433.
56 Bérenger, J.P., 1994. A perfectly matched layer for the absorption of electromagnetic waves,
57 *Journal of Computational Physics*, 114(2), 185-200.
58 Bindel, D.S. & Govindjee, S., 2005. Elastic PMLs for resonator anchor loss simulation,
59 *International Journal for Numerical Methods in Engineering*, 64(6), 789-818.
60

- 1
2
3 Carcione, J.M., 2015. *Wave Fields in Real Media: Wave Propagation in Anisotropic,*
4 *Anelastic, Porous and Electromagnetic Media*, Elsevier.
- 5 Cerjan, C., Kosloff, D., Kosloff, R., & Reshef, M., 1985. A nonreflecting boundary condition
6 for discrete acoustic and elastic wave equations, *Geophysics*, 50(4), 705-708.
- 7 Cervený, V., 2005. *Seismic ray theory*, Cambridge University Press.
- 8 Collino, F. & Tsogka, C., 2001. Application of the perfectly matched absorbing layer model
9 to the linear elastodynamic problem in anisotropic heterogeneous media, *Geophysics*,
10 66(1), 294-307.
- 11 Deuss, A., Irving, J.C. & Woodhouse, J.H., 2010. Regional variation of inner core anisotropy
12 from seismic normal mode observations, *Science*, 328(5981), 1018-1020.
- 13 Diez, A. & Eisen, O., 2015. Seismic wave propagation in anisotropic ice-Part 1: Elasticity
14 tensor and derived quantities from ice-core properties, *The Cryosphere*, 9(1), 367-384.
- 15 Dmitriev, M.N. & Lisitsa, V.V., 2011. Application of M-PML reflectionless boundary
16 conditions to the numerical simulation of wave propagation in anisotropic media. Part I:
17 Reflectivity, *Numerical analysis and Applications*, 4(4), 271-280.
- 18 Duru, K. & Kreiss, G., 2014. Numerical interaction of boundary waves with perfectly
19 matched layers in two space dimensional elastic waveguides, *Wave Motion*, 51(3),
20 445-465.
- 21 Fathi, A., Poursartip, B., & Kallivokas, L.F., 2015. Time-domain hybrid formulations for
22 wave simulations in three-dimensional PML-truncated heterogeneous media,
23 *International Journal for Numerical Methods in Engineering*, 101, 165-198.
- 24 Festa, G. & Vilotte, J. P., 2005. The Newmark scheme as velocity–stress time-staggering: an
25 efficient PML implementation for spectral element simulations of elastodynamics,
26 *Geophysical Journal International*, 161(3), 789-812.
- 27 Gao, K. & Huang, L., 2017. Optimal damping profile ratios for stabilization of perfectly
28 matched layers in general anisotropic media, *Geophysics*, 83(1), T15-T30.
- 29 Halpern, L., Petit-Bergez, S., & Rauch, J., 2011. The analysis of matched layers, *Confluentes*
30 *Mathematici*, 3(02), 159-236.
- 31 Komatitsch, D., Barnes, C. & Tromp, J., 2000. Simulation of anisotropic wave propagation
32 based upon a spectral element method, *Geophysics*, 65(4), 1251-1260.
- 33 Komatitsch, D. & Martin, R., 2007. An unsplit convolutional perfectly matched layer
34 improved at grazing incidence for the seismic wave equation, *Geophysics*, 72(5),
35 SM155-SM167.
- 36 Komatitsch, D. & Tromp, J., 1999. Introduction to the spectral element method for
37 three-dimensional seismic wave propagation, *Geophysical journal international*, 139(3),
38 806-822.
- 39 Komatitsch, D. & Tromp, J., 2003. A perfectly matched layer absorbing boundary condition
40 for the second order seismic wave equation, *Geophysical Journal International*, 154(1),
41 146-153.
- 42 Li, Y. & Bou Matar, O., 2010. Convolutional perfectly matched layer for elastic second order
43 wave equation, *The Journal of the Acoustical Society of America*, 127(3), 1318-1327.
- 44 Liao, Z.P., Wong, H.L., Yang, B.P. & Yuan, Y.F., 1984. A transmitting boundary for
45 transient wave analysis, *Science in China Series A-Mathematics Physics Astronomy &*
46 *Technological Science*, 27(10), 1063–1076.
- 47 Liu, H., & Zhang, H., 2019. Reducing computation cost by Lax-Wendroff methods with
48 fourth order temporal accuracy, *Geophysics*, 84(3), T109-T119.
- 49 Ma, S. & Liu, P., 2006. Modeling of the perfectly matched layer absorbing boundaries and
50 intrinsic attenuation in explicit finite-element methods, *Bulletin of the Seismological*
51 *Society of America*, 96(5), 1779-1794.
- 52 Martin, R., Komatitsch, D. & Gedney, S.D., 2008. A variational formulation of a stabilized
53 unsplit convolutional perfectly matched layer for the isotropic or anisotropic seismic
54 wave equation, *Comput. Model. Eng. Sci*, 37(3), 274-304.
- 55 Matuszyk, P.J. & Demkowicz, L.F., 2013. Parametric finite elements, exact sequences and
56 perfectly matched layers, *Computational Mechanics*, 51(1), 35-45.
- 57 Meza-Fajardo, K.C. & Papageorgiou, A.S., 2008. A nonconvolutional, split-field, perfectly
58
59
60

- 1
2
3 matched layer for wave propagation in isotropic and anisotropic elastic media: stability
4 analysis, *Bulletin of the Seismological Society of America*, 98(4), 1811-1836.
- 5 Moczo, P., Kristek, J., Vavrycuk, V., Archuleta, R.J. & Halada, L., 2002. 3D heterogeneous
6 staggered-grid finite-difference modeling of seismic motion with volume harmonic and
7 arithmetic averaging of elastic moduli and densities, *Bulletin of the Seismological*
8 *Society of America*, 92(8), 3042-3066.
- 9 Ping, P., Zhang, Y. & Xu, Y., 2014. A multiaxial perfectly matched layer (M-PML) for the
10 long-time simulation of elastic wave propagation in the second order equations, *Journal*
11 *of Applied Geophysics*, 101, 124-135.
- 12 Ping, P., Zhang, Y., Xu, Y. & Chu, R., 2016. Efficiency of perfectly matched layers for
13 seismic wave modeling in second order viscoelastic equations, *Geophysical Journal*
14 *International*, 207(3), 1367-1386.
- 15 Savage, M.K., 1999. Seismic anisotropy and mantle deformation: what have we learned from
16 shear wave splitting? *Reviews of Geophysics*, 37(1), 65-106.
- 17 Sayers, C.M., 2018. Elastic anisotropy of polycrystalline ice with transversely isotropic and
18 orthotropic symmetry, *Geophysical Journal International*, 215(1), 155-164.
- 19 Semblat, J. F., Lenti, L., & Gandomzadeh, A., 2011. A simple multi-directional absorbing
20 layer method to simulate elastic wave propagation in unbounded domains, *International*
21 *Journal for Numerical Methods in Engineering*, 85(12), 1543-1563.
- 22 Stacey, R., 1988. Improved transparent boundary formulations for the elastic-wave
23 equation, *Bulletin of the Seismological Society of America*, 78(6), 2089-2097.
- 24 Sochacki, J., Kubichek, R., George, J., Fletcher, W. R., & Smithson, S., 1987. Absorbing
25 boundary conditions and surface waves, *Geophysics*, 52(1), 60-71.
- 26 Xie, Z.N., Komatitsch, D., Martin, R. & Matzen, R., 2014. Improved forward wave
27 propagation and adjoint-based sensitivity kernel calculations using a numerically stable
28 finite-element PML, *Geophysical Journal International*, 198(3), 1714-1747.
- 29 Xie, Z.N., Matzen, R., Cristini, P., Komatitsch, D. & Martin, R., 2016. A perfectly matched
30 layer for fluid-solid problems: Application to ocean-acoustics simulations with solid
31 ocean bottoms, *The Journal of the Acoustical Society of America*, 140(1): 165-175.
- 32 Xie, Z.N. & Zhang, X.B., 2017. Weak-form time-domain perfectly matched layer, *Chinese*
33 *Journal of Geophysics*, 60(10), 3823-3831.
- 34 Zeng, C., Xia, J., Miller, R. D., & Tsoflias, G. P., 2011. Application of the multiaxial
35 perfectly matched layer (M-PML) to near-surface seismic modeling with Rayleigh
36 waves. *Geophysics*, 76(3), T43-T52.
- 37 Zhang, W. & Shen, Y., 2010. Unsplit complex frequency-shifted PML implementation using
38 auxiliary differential equations for seismic wave modeling, *Geophysics*, 75(4),
39 T141-T154.
- 40 Zhebel, E., Minisini, S., Kononov, A. & Mulder, W.A., 2014. A comparison of continuous
41 mass-lumped finite elements with finite differences for 3-D wave propagation,
42 *Geophysical Prospecting*, 62(5), 1111-1125.
- 43 Zhu, H., Komatitsch, D. & Tromp, J., 2017. Radial anisotropy of the North American upper
44 mantle based on adjoint tomography with USArray, *Geophysical Journal*
45 *International*, 211(1), 349-377.
- 46 Zhu, T., 2017. Numerical simulation of seismic wave propagation in viscoelastic-anisotropic
47 media using frequency-independent Q wave equation, *Geophysics*, 82(4), WA1-WA10.
- 48
49
50
51
52
53
54
55
56
57
58
59
60

Table 1. M-PML formulations and number of additional variables needed for their implementation in time-domain elastodynamics (in-plane wave)

| | first order | second order |
|---------|---|--|
| split | Meza-Fajardo & Papageorgiou (2008) [#] ; 10 [#] | Ping et al. (2014, 2016) [#] ; 10 [#] |
| | Gao & Huang (2017) [#] ; 10 | |
| unsplit | Martin et al. (2008) [*] ; 8 [*] | Li & Bou (2010) ^{**} ; 8 [#] (8 [*]) |
| | Gao & Huang (2017) [*] ; 8 [*] | Fathi et al. (2015) [#] ; 6 [#] |
| | | This paper ^{**} ; 4 [#] (8 [*]) |

(# or * denotes the use of a frequency-shifted or classical coordinate stretching function)

Table 2. Geometrical and discretization parameters for the homogeneous isotropic semi-infinite model and anisotropic infinite model

| | Isotropic | Anisotropic medium III, IV | Apatite |
|-------------------------------|--|-------------------------------|-----------------------|
| | | Physical domain dimension | |
| Length | 11km | 8m | 25cm |
| Width | 4km | 8m | 25cm |
| | | Physical domain properties | |
| Density | 2700kg/m ³ | 1kg/m ³ | 3200kg/m ³ |
| Elastic coefficients | $V_p=3200\text{m/s}$, $V_s=1870\text{m/s}$. | Given by Table 3 | Given by Table 3 |
| | | Source location | |
| From left boundary | 0.25km | 4m | 12.5cm |
| From bottom boundary | 3.75km | 4m | 12.5cm |
| | | Receiver location | |
| From left boundary | 9.8km | 5m | 22.5cm |
| From bottom boundary | 4km | 6m | 20.5cm |
| | | Ricker wavelet parameters | |
| Dominant frequency | 2.5Hz | 1Hz | 170kHz |
| Onset time | 0.4s | 0.5s | 5.88 μs |
| | | Discretization parameters | |
| Element size | 0.1km | 0.25m | 0.25cm |
| Layer of elements used in PML | 3, 9, 15 | 9 | 9 |
| Time step | 0.0004s | 0.001s | 0.02 μs |
| Total duration | 20s | 100s | 2000 μs |

Table 3. Elasticity coefficients of an anisotropic medium

| Elasticity coefficients (N/m ²) | III | IV | Apatite |
|---|-----|----|----------|
| c_{11} | 4 | 10 | 1.65e+11 |
| c_{22} | 20 | 20 | 6.20e+10 |
| c_{66} | 2 | 6 | 3.96e+10 |
| c_{12} | 7.5 | 2 | 5.00e+10 |

Table 4. Media properties of the adapted layered model from [Zhu \(2017\)](#)

| Layers | Thickness | V_P (m/s) | V_S (m/s) | ρ (kg/m ³) | c_{11} (N/m ²) | c_{22} (N/m ²) | c_{66} (N/m ²) | c_{12} (N/m ²) |
|--------|-----------|----------------|----------------|--------------------------------|---------------------------------|---------------------------------|---------------------------------|---------------------------------|
| 1 | 300m | 1900 | 1200 | 1800 | | | | |
| 2 | 250m | | | 2300 | 2.33e+10 | 1.32e+10 | 2.78e+9 | 6.56e+9 |
| 3 | 150m | | | 2200 | 1.35e+10 | 1.98e+10 | 8.8e+9 | 1.04e+10 |
| 4 | | 3200 | 1500 | 2500 | | | | |

Table 5. Geometrical and discretization parameters for the adapted layered model from [Zhu \(2017\)](#)

| Truncated computational domain dimension | | Receiver location | | Discretization parameters | |
|--|-------|---------------------------|------|-------------------------------|---------|
| Length | 1000m | From left boundary | 900m | Polynomial degree of SE | 5 |
| Width | 1000m | From bottom boundary | 100m | Element size | 10m |
| Source location | | Ricker wavelet parameters | | Layer of elements used in PML | 9 |
| From left boundary | 300m | Dominant frequency | 10Hz | Timestep | 0.0002s |
| From bottom boundary | 900m | Onset time | 0s | Total duration | 20s |

Reponses to the reviewers and editorial office**Multi-axial unsplit frequency-shifted perfectly matched layer for displacement-based anisotropic wave simulation in infinite domain****Referee: 1**

Comment 1.1: The development of seismic hazard analysis on basis of deterministic wave simulation methods become more and more important in particular for region lack of abundant earthquake records.

Response: Thank you so much for your comment. We fully agree the importance of developing deterministic wave simulation method for seismic hazard analysis. Thus, we add some sentences in conclusion section.

Comment 1.2: PML is one of the key components in displacement-based deterministic wave simulation, acting as a highly accurate approximation of the infinite-domain.

Response: Thank you so much for your comment.

Comment 1.3: This paper addressed the construction of long-time stable multi-axial unsplit frequency-shifted PML(M-UFSPM) for wave propagation in infinite anisotropic media. It is shown clearly in this paper the derivation of M-UFSPML using the frequency-shifted stretching technique coupling with a non-rigorous chain rule. Moreover, it is show clearly that the resulted M-UFSPML are better performed than M-PML in absorption of near-grazing incident wave and low frequency incident waves. The authors validated the accuracy and long-time numerical stability of their M-UFSPML implementation in spectral element methods with classical numerical examples. Overall, the work presented in this paper is original, and has important academic and practical value.

Response: We would like to express our sincere thanks to the reviewer for the recognition of the topic of this article and our work.

Comment 1.4: This paper is also well organized and its presentation is good. The quality of English language is generally good. However, there are a few expressions and terms that could be better reformulated in English, for more clarity to the reader.

Response: Thank you so much for your kind suggestion. We admit that the expression is poor in original version. We spent a lot time on revising our paper to improve the expression and make it clearer to the reader.

Referee: 2

This paper developed a time-domain Multi-axial unsplit frequency-shifted PML (M-UFSPML) approach for analyzing the wave propagation problems in the infinite domains. In this regard, an anisotropic wave simulation based on second order wave equation was implemented by displacement numerical approach. Finally, the accuracy of the proposed formulation was investigated by solving some practical examples. The presented work is good and the results are new.

Response: We would like to express our sincere thanks to the reviewer for the recognition of the topic of this article and our work. We have modified our paper according to your following comments.

Comment 2.1: However there are several issues that must be addressed by the authors before the paper is to be accepted. These comments are listed as follows: This paper analyzes good examples. But they are small and have little degree of freedom (DOF). With these examples, the efficiency of the proposed method cannot be evaluated. By solving another example with a high degree of freedom, authors should demonstrate the efficiency of the method as well as the power of the formulation.

Response: Thank you so much for your suggestion. Except the Coupled isotropic and anisotropic wave simulation in a layered model, the problems selected in our paper is almost the same as that in Meza-Fajardo & Papageorgiou (2008) in order for direct comparison of the first-order M-PML to our M-UFSPML. The degree of freedom is small, but we show clearly the improvement of M-UFSPML due to less memory variables are needed. Thank you again for your comment. We would like to do this kind of work after the parallel implementation of M-UFSPML, which is under investigation. Otherwise, the one core implementation restrict the degree of freedom and is less meaningful for efficiency demonstration.

Comment 2.2: In the presented examples, the wave is assumed as vertical incident waves. Is the proposed method capable to analyze the inclined waves? This issue can be shown in the prepared additional example (Comment 1).

Response: Thank you so much. No restrictions on the type of waves are needed for our M-UFSPML. For source locating inside the computational region, truncated by M-UFSPML, almost the same absorption efficiency can be achieved irrespective of the incident angle. Even for near-grazing incident waves, the absorption of our M-UFSPML are shown as quite good.

Comment 2.3: All the results of the presented work are obtained in the time-domain. In general, to validate and compare the amplitude of responses, the results can also be displayed in the frequency-domain. Is there this capability for the results of research?

Response: Thank you for your comments. Unlike scattering problem, the simulation of seismic wave radiating from finite-fault are generally setup in time-domain. The results obtained in this paper can also be extended into wave simulation in frequency-domain.

Comment 2.4: As presented in the paper, the proposed approach has the ability to reduce the

1
2
3 **volume of calculations. This issue needs to be tested by presenting analysis time compared to**
4 **other methods.**

5
6 Response: Thank you so much. Indeed, we have already compared with our M-UFSPML to M-
7 USFMPL-Li and Stacey ABC. The absorbing efficiency of our M-UFSPML are better than M-
8 USFMPL-Li and much better than Stacey ABC, which is favored by engineers due to its simple
9 implementation. A simple time comparison could be misleading unless given a community model.
10 Thus, according to your comment, we would like to setup a community model for precise
11 comparison
12

13
14
15 **Comment 2.5: The titles of the sections of the paper are too long. These need to be shortened.**

16 Response: You are right, we shortened.
17

18
19 **Comment 2.6: The conclusion part of the manuscript is very poorly interpreted. This section**
20 **needs to be reviewed and the results better displayed.**

21 Response: Thank you so much. Yes, the conclusion part in original version is too short. we have
22 rewritten our conclusion.
23

24
25 **Comment 2.7: The paper requires an extensive editorial work.**

26 Response: We admit that the expression is poor in original version. We spent a lot time on revising
27 our paper to improve the expression and make it clearer to the reader.
28

29
30 **Comment 2.8: Some references in analyzing wave propagation problems by novel numerical**
31 **methods (such as time-domain boundary element method) are missed. Here are some papers**
32 **the authors should have known:**

33 - Panji, M., Kamalian, M., Asgari Marnani, J. and Jafari, M., K. (2013)" Transient analysis
34 of wave propagations problems by half-plane BEM", *Geophysical Journal International*, 194,
35 1849-1865.
36

37 - Panji, M., Kamalian, M., Asgari Marnani, J. and Jafari, M., K., (2014)" Analyzing seismic
38 convex topographies by a half-plane time-domain BEM", *Geophysical Journal International*,
39 197(1), 591-607.
40

41 - Panji, M. and Ansari, B., (2017). "Transient SH-wave scattering by the lined tunnels
42 embedded in an elastic half-plane", *Engineering Analysis with Boundary Elements*, 84, 220-
43 230.
44

45 - Panji, M., Mojtazadeh-Hasanlouei, S. and Yasemi, F. (2020). "A half-plane time-domain
46 BEM for SH-wave scattering by a subsurface inclusion", *Computers & Geosciences*, 134, 1-
47 19.
48

49 - Panji, M. and Habibivand, M., (2020). "Seismic analysis of semi-sine shaped alluvial hills
50 above subsurface circular cavity", *Earthquake Engineering & Engineering Vibration*, 19,
51 903-917.
52

53 Response: Thank you so much. I have added one of above paper as references. The modification let
54 me to think about to setup a community model for precise comparison of accuracy and
55 computational efficiency for difference infinite domain truncation techniques. I hope this kind of
56 work do give the guidelines of the choice of infinite-domain truncation technique to meet the
57 different requirement of users.
58
59
60

Editorial office

Thank you so much for your hard work and patience. We have modified our paper carefully according to the nice comments of the two reviewers. We do not show the detail modification with colors since there are too much due to our poor English. However, we uploaded a file to show the difference between the original and modified version. We hope our modifications can meet your expectation.

For Review Only